Atomic structure of an Al–Co–Ni decagonal quasicrystalline surface

J. Yuhara,[1,]* J. Klikovits,[2] M. Schmid,[2] P. Varga,[2] Y. Yokoyama,[3] T. Shishido,[4] and K. Soda[5]

[1]*Department of Physical Science and Engineering, School of Engineering, Nagoya University, Furo-cho, Chikusa-ku, Nagoya, 464-8603, Japan*

[2]*Institut für Allgemeine Physik, Technische Universität Wien, Wiedner Hauptstraße 8-10, A-1040 Wien, Austria*

[3]*Faculty of Engineering, Himeji Institute of Technology, Shosha, Himeji 671-2201, Japan*

[4]*Institute for Materials Research, Tohoku University, Sendai 980-8577, Japan*

[5]*Department of Crystalline Materials Science, School of Engineering, Nagoya University, Furo-cho, Chikusa-ku, Nagoya, 464-8603, Japan*

We have analyzed the structure and composition of the first layer of an $Al_{72}Co_{16}Ni_{12}$ tenfold surface by means of scanning tunneling microscopy (STM), ion scattering spectroscopy (ISS), and Auger electron spectroscopy (AES). High-resolution STM images reveal local structures that have decagonal symmetry in addition to the usual pentagonal symmetry of the surface. This quasicrystal surface resembles a random tiling instead of an ideal quasiperiodic tiling. After annealing at 1100 K, the total surface atomic density found by ISS is $(9\pm1)\times10^{14}$ cm^{-2}. The surface densities of Al and TM (transition metal, i.e., Co and Ni) are determined as $(8\pm1)\times10^{14}$ cm^{-2} and $(1.0\pm0.2)\times10^{14}$ cm^{-2}, respectively from ISS, indicating a similar density of Al and much lower density of the TM atoms in the surface layer than in a truncated bulk. The Al surface atomic density agrees well with the number of corrugation maxima in the STM images. A model of the arrangement of the Al atoms in the top layer is presented. Scanning tunneling spectroscopy (STS) is performed to study the local electronic structure. The STS spectrum at the corrugation maxima is similar to that at the corrugation minima. A few ≈0.12 nm high protrusions in the STM images are attributed to local oxide clusters due to their STS spectra different from the corrugation maxima and through *in situ* STM observations during exposure to O_2 gas at 2×10^{-6} Pa at RT.

I. INTRODUCTION

The surfaces of quasicrystals (QCs) have been studied intensively over the past few years after large single-grain QC samples, such as Al–Co–Cu, Al–Cu–Fe, Al–Pd–Mn, Al–Co–Ni, etc., became available.[1–4] A decagonal Al–Co–Ni quasicrystal (QC) was discovered in 1989 by Tsai *et al.* as a thermodynamically stable phase.[5] The floating zone method and the Czochralski method were successfully applied to produce single grains of Al–Co–Ni quasicrystals,[6,7] although the Al content at the end of the QC slightly increases because of the Al enrichment of the melt during off-stoichiometric growth.[8] The bulk atomic structure of Al–Co–Ni quasicrystals has been studied intensively by high-resolution transmission electron microscopy (TEM),[9,10] high-angle dark-field scanning transmission electron microscopy (HAADF-STEM),[11] and x-ray and electron diffraction.[12,13] The quasicrystalline phases have clearly shown an ordered arrangement of columnar atom clusters, which have a decagonal shape with pentagonal symmetry and a diameter of 2.0 nm.[9] The columnar clusters forming pentagonal antiprismatic channels were identified by x-ray scattering experiments.[12] Recently, the surface structure of the Al–Co–Ni decagonal quasicrystalline surface has also been studied.[14–19] From low energy electron diffraction (LEED) and scanning tunneling microscopy (STM) studies, it is reported that there is only one type of monoatomic step on the tenfold surface with a step height of 0.2 nm.[14,15] The symmetry of each layer is not decagonal but pentagonal and two adjacent layers are related by inversion symmetry.[15] The

elemental concentrations of the cleaved and annealed $Al_{72}Co_{12}Ni_{16}$ surface (i.e., more on the Ni-rich side than our sample) have been investigated by Auger electron spectroscopy (AES), and it was found that heat-treatments of these cleaved quasicrystal surfaces show no large changes in chemical composition up to 1050 K, indicating that the composition of the near-surface layers is stable up to this temperature.[17] Many aspects important for understanding the surface properties and structure of AlCoNi quasicrystals, such as the surface atomic density, first-layer concentrations and their relation to the structure, have not been studied yet.

In this paper, the geometric and local electronic structure as well as the surface concentrations and atomic densities of a tenfold surface of $Al_{72}Co_{16}Ni_{12}$ are studied by high-resolution STM, scanning tunneling current-voltage spectroscopy (STS), ion scattering spectroscopy (ISS), and AES.

II. EXPERIMENT

The specimen used in the present experiment was a decagonal $Al_{72}Co_{16}Ni_{12}$ single-grain QC prepared by the Czochralski method. It was identified to be the Co-rich decagonal phase by transmission electron diffraction. The details of the bulk structure of the specimen are described in Ref. 7. A decagonal surface of the specimen was prepared in an ultra-high vacuum (UHV) chamber with a base pressure below 1 $\times10^{-8}$ Pa by cycles of 2 keV Ar$^+$ sputtering at room temperature followed by annealing at temperatures up to 1150 K. The annealing was performed by electron bombard-

ment of the sample holder at an emission current of 10–20 mA and a voltage of 600–900 V. The temperature of the specimen was monitored by a thermocouple fixed to the nontransferable part of the sample holder. The tenfold symmetry of the surface was confirmed with the LEED pattern. The cleanliness of the $Al_{72}Co_{16}Ni_{12}$ surface was measured by AES after sputtering and annealing; no contaminations such as C and O could be observed on the QC surface within the detection limits.

STM experiments were performed in an UHV chamber equipped with a customized Omicron room-temperature micro-STM, two-grid LEED optics, a cylindrical mirror analyzer with coaxial electron gun for AES, an ion source and hemispherical analyzer for ISS, and a mass spectrometer for residual gas analysis. The base pressure of this chamber is below 5×10^{-9} Pa. A titanium sublimation pump with a liquid-nitrogen cooled cryopanel was further used to reduce the surface contaminations such as oxygen during analysis. All STM images were obtained in constant current mode with negative sample bias voltage. STS spectra were obtained together with the simultaneous STM measurements by numerical differentiation at each pixel and averaging over 20 equivalent sites to reduce noise.

The surface densities (atoms per unit area) and first-layer concentrations of Al and TM (transition metal, i.e., combined signal of Co and Ni) were determined by the ISS signal compared to that of an AlNi(110) standard sample which was cleaned by cycles of 2 keV Ar^+ sputtering at room temperature followed by annealing at a temperature of 1150 K resulting in surface concentrations of 50% Al and 50% Ni.[20] Here, the peak areas after subtraction of the background were used for the estimation of the surface atomic densities. In the ISS experiments, a 1 keV He^+ ion beam was incident at the angle of 45° and the scattered He^+ ions were detected at the scattering angle of 90°. In this geometry, neither shadowing, blocking, nor neutralization by the neighboring atoms affect the calibration with the AlNi(110) surface, since its buckling amplitude is only 0.02 nm.

The elemental concentrations in the surface were also studied by AES. Again, we have used the stoichiometric AlNi(110) surface as a standard for the calibration of the Ni/Al ratio, while we have determined the Co/Ni ratio using sensitivity factors in the literature[21] for the Ni LMM(848 eV) and Co LMM(656 eV) peak-to-peak heights. For Al, we have used the Auger peak at 68 eV(LMM) rather than the peak 1396 eV because of its almost 5 times higher surface sensitivity and higher signal intensity. It has been noted that quantitative Auger analysis of quasicrystals is far from trivial since the use of atomic sensitivity factors derived from pure elements of other alloys can lead to large errors of the concentrations.[22] The Auger results should therefore be seen more as indicators of the qualitative trends and as a check for any anomalous Co/Ni ratio (which is not accessible by ISS) than as accurate measurements of the absolute values of the concentrations.

III. RESULTS

This section is separated into three subsections. In the first subsection, we present the results related to the atomic struc-
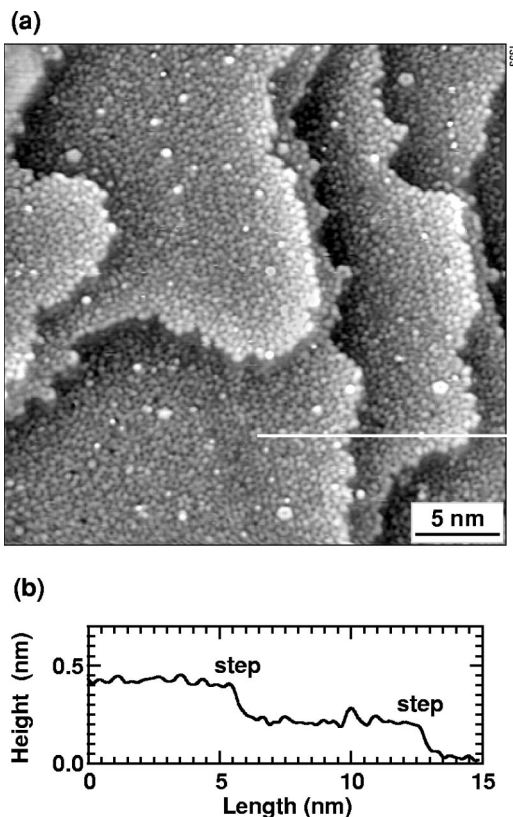

FIG. 1. (a) STM image of the $Al_{72}Co_{16}Ni_{12}$ surface (30 $\times$ 30 nm^2; $I=0.5$ nA, $V=-0.8$ V). For better contrast, a high-pass filter has been applied, leading to bright appearance of the step edges. (b) Section profile along the white line in (a).

ture of the $Al_{72}Co_{16}Ni_{12}$ surface. The second subsection addresses the surface atomic density and composition. In the last subsection, the surface oxidation and STS results on the local electronic structure are described.

A. Atomic structure

Figure 1 shows a typical STM image of the $Al_{72}Co_{16}Ni_{12}$ surface. All steps have 0.2 nm in height (monoatomic step), in agreement with the previous reports.[14,15] There is no annealing temperature dependence observed in the STM images between 800 K and 1150 K except the decay of the sputter-induced roughness with temperature.

The rotational symmetry of the surface is examined by LEED, which reveals the tenfold symmetry, as shown in Fig. 2(a). The LEED pattern observed here is consistent with the LEED pattern measured by the spot profile analysis low energy electron diffraction (SPA-LEED).[14] From the STM image (Fig. 1), a fast Fourier transform (FFT) image and an autocorrelation function (ACF) are extracted to examine the symmetry, as shown in Figs. 2(b) and 2(c), respectively. The FFT image shows the tenfold symmetry, and nicely corresponds to the LEED pattern (a), except for the inner spots whose k-vector is about 10.5 nm^{-1}. These spots are invisible in the LEED pattern shown in Fig. 2(a) and only appear in LEED at an incident electron energy less than 40 eV. Both LEED and FFT images have outermost spots rotated by 18°
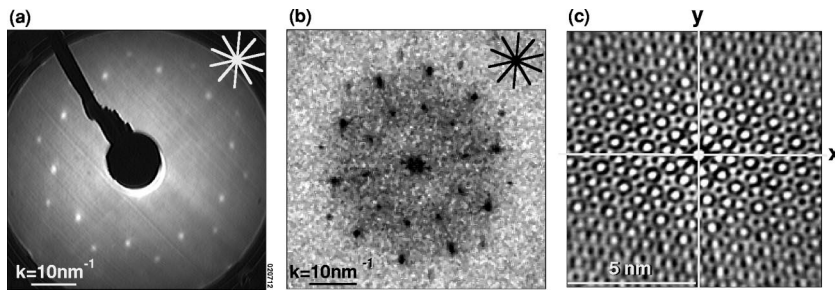
FIG. 2. (a) LEED pattern of the $Al_{72}Co_{16}Ni_{12}$ surface at 46 eV incident electron energy. (b) Fourier transform of Fig. 1(a) displayed with logarithmic greyscale. (c) Autocorrelation function of Fig. 1(a).

at the k-vector of 20.7 nm^{-1}, in good agreement with the (1000) beam found by SPA-LEED (20.1 nm^{-1}, Ref. 14). These were the largest spatial frequencies observed in our LEED and FFT images. The corresponding atomic row distance in real space is 0.30 nm. The ACF is a spatial map of the pair-correlation function.[2,3] The correlation maxima are visible even close to the edges, indicating a strong spatial correlation extending over distances of at least ±5 nm. According to Gierer *et al.*, the correlation length of the perfect quasicrystalline order is reported to be more than 3 nm.[14] Therefore, the resolution of our STM images is high enough to examine the detailed atomic structure.

Figures 3(a)–3(e) show high-resolution STM images of the $Al_{72}Co_{16}Ni_{12}$ surface. We can clearly see different sizes of arrangements of fivefold symmetry, not only pentagons formed by maxima (protrusions) but also by minima (depressions), as shown by circles A–D in Fig. 3 and by larger units (circle E). The distance between the protrusions in the smallest pentagonal rings (type "A") is 0.32 ± 0.02 nm, and the atoms are considered to be located at these protrusion maxima. The outermost spots (20.7 nm^{-1}) in the LEED and FFT images where atomic row distance in real space is 0.30 nm correspond to this interatomic distance $(0.30/\cos 18° =0.32)$. The distance between the protrusions in the next smallest rings (type "B") is 0.5 ± 0.1 nm, which corresponds to the inner spots in the LEED and FFT images. In circle C, three sizes of pentagonal rings formed by maxima, minima, and maxima, respectively, are observed, which is similar to the pattern reported by Kishida *et al.*[15] The inner pentagon of this structure has the same size and orientation as type "A." In circle D, there is a maximum in the center, and at least two sizes of pentagonal rings formed by minima and maxima are observed. The distance between the minima in circles C is the same as the distance between

the maxima in circle B, and also the orientation of these pentagons is the same.

Furthermore, we can observe almost symmetrical rings with ten maxima and/or minima as shown by circles F and G in Fig. 3. Therefore, the $Al_{72}Co_{16}Ni_{12}$ surface forms local tenfold rings in addition to the fivefold structures. The cluster size of these tenfold rings is about 2 nm, which is consistent with the bulk cluster size observed in TEM.[9] Moreover, a larger ring with 20 protrusions is observed as shown in circle K. There are maxima shaped round, star, pentagon, and local minima as shown in circles G–J. These local maxima and minima are usually located at the center of larger rings with 5 or 10 protrusions. The center of the star shaped pattern in circle J is always about 0.10 nm lower than surrounding maxima. Similarly, the centers of local maxima in circles H and I are about 0.10–0.12 nm higher than surrounding maxima. Although the orientation of structures of the same size and shape is usually the same, we sometimes observe fivefold structures with opposite orientation in the same terrace as shown by circle L. Assuming that all hardly resolvable rings of type A consist of five protrusions, the number of protrusions observed in the STM images was determined as $(8\pm1)\times10^{14}$ cm^{-2}.

B. Surface composition

Figure 4 shows ISS spectra of the $Al_{72}Co_{16}Ni_{12}$ surface after sputtering (a) and after annealing at 1100 K (b) as well as the spectrum of the stoichiometric AlNi(110) surface as a reference (c). In Figs. 4(a) and 4(b), the Al peak is clearly seen, but the Ni and Co peaks overlap because of the similarity of their atomic numbers and masses. We define the TM (transition metal) signal as the sum of the Ni and Co signals, since the Co scattering cross-section is very close to (only
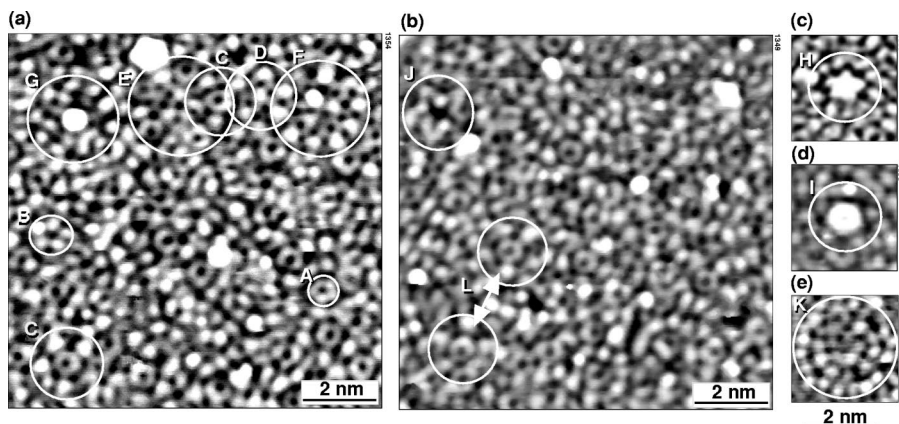

FIG. 3. High-resolution STM images of the $Al_{72}Co_{16}Ni_{12}$ surface (I=0.5 nA, $V=-0.5$V). Different sizes of pentagonal structure elements and other features are marked by circles A–L (see text).
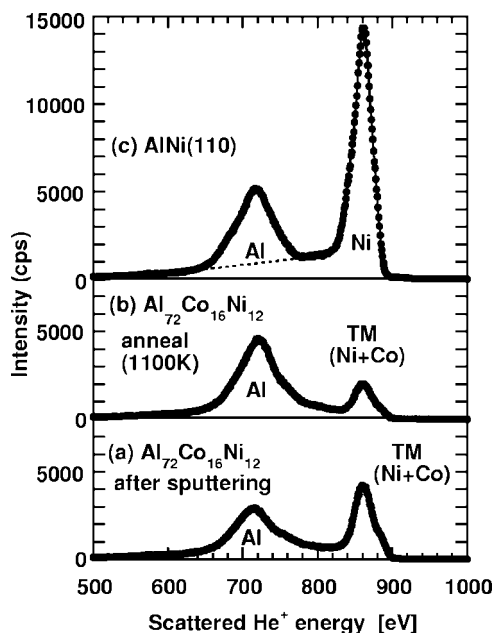
FIG. 4. ISS spectra of the $Al_{72}Co_{16}Ni_{12}$ surface (a) after sputtering and (b) after annealing at 1100 K, and (c) of the stoichiometric AlNi(110) surface as reference.

$\approx 3\%$ lower than) the Ni scattering cross section.[23] By assuming both scattering cross sections to be equal, the surface concentration ratios of Al: TM after sputtering and after annealing at 1100 K are estimated to be 74%: 26%, and 90%: 10%, respectively. Thus, the first-layer composition after sputtering is similar to the QC bulk composition, and the Al surface concentration increases during annealing. By comparing the absolute count rates of the QC surface and the AlNi(110) standard, the surface densities of Al and TM after annealing can be determined as $(8\pm1)\times10^{14}$ cm^{-2} and $(1\pm0.2)\times10^{14}$ cm^{-2}, respectively. The Al surface atomic density roughly agrees with the number of maxima observed in the STM images.

Figure 5 shows the annealing temperature dependence of the elemental concentrations of the $Al_{72}Co_{16}Ni_{12}$ surface and near-surface layers measured by AES. To obtain each point
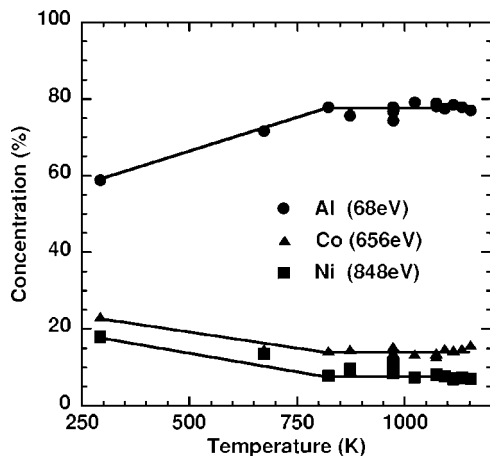

FIG. 5. Annealing temperature dependence of the surface composition of $Al_{72}Co_{16}Ni_{12}$ measured by AES.

of data, the QC was sputtered and annealed, and then the AES spectrum was measured at RT. The Al concentration is reduced by the preferential sputtering but increased by annealing. Above the annealing temperature of 800 K, the surface concentrations determined by AES do not change at all. Since AES probes a few monolayers and ISS detects the first layer only, the Al concentration measured by AES becomes lower than that measured by ISS and closer to the composition of the $Al_{72}Co_{16}Ni_{12}$ bulk. The Co/Ni concentration ratio measured by AES increases upon annealing; if we assume that this ratio reflects the true surface concentrations we can use it to determine the contributions of Co and Ni to the TM signal in the ISS spectra of the annealed surface. This results in surface atomic densities of $(0.6\pm0.2)\times10^{14}$ cm^{-2} for Co and $(0.4\pm0.2)\times10^{14}$ cm^{-2} for Ni. As menitoned in Sec. II, we must keep in mind that the error bars of the AES data are rather large, thus our data are not accurate enough to conclude that the Co/Ni ratio at the surface surface deviates from the bulk stoichiometry.

C. Oxidation and electronic structure

Figures 6(a)–6(d) show STM images before and after exposure of the QC surface to O_2 gas at 2×10^{-6} Pa at RT for 1, 3, and 6 min, respectively. The number of bright protrusions with a height of approximately 0.12 nm increases with time, as shown in Fig. 6 (circles). The number of these protrusions also increased during the STM measurements at the base pressure below 5×10^{-9} Pa (and an O_2 partial pressure below 1×10^{-10} Pa) in a few hours. Moreover, the O *KLL* peak-to-peak height in the Auger spectra increases after these treatments, as shown in Figs. 6(e) and 6(f). Thus, the protrusions are somehow related to oxygen, most likely to small oxide clusters. To examine the details of local electronic structure of the QC surface, STS measurements were performed. Figure 7 shows averaged STS spectra from the $Al_{72}Co_{16}Ni_{12}$ surface at the corrugation maxima (circles) and minima (squares) of the clean surface, as well as at the protrusions attributed to oxide clusters (triangles). The STM image during the STS measurement is shown in the inset of Fig. 7. All spectra of the clean surface are very similar to each other, independent of the exact location (maxima or minima of the apparent height). By comparison, the density of state (DOS) at the "oxide" protrusions is much lower at energies above the Fermi level, indicating that these protrusions consist of a different material.

IV. DISCUSSION

Concerning the surface composition, we find by AES that preferential sputtering leads to Al depletion in the near-surface region ("altered layer") as already observed for an $Al_{70}Co_{15}Ni_{15}$ quasicrystal[16] and also for the similar AlCuFe system.[24] At first glance, the bulklike composition of the first layer of the sputtered surface found by ISS may seem inconsistent with the AES result, but it should be mentioned that ion-induced mobility will lead to segregation within the altered layer even at room temperature, leading to a higher concentration of the element with lower surface energy (Al)
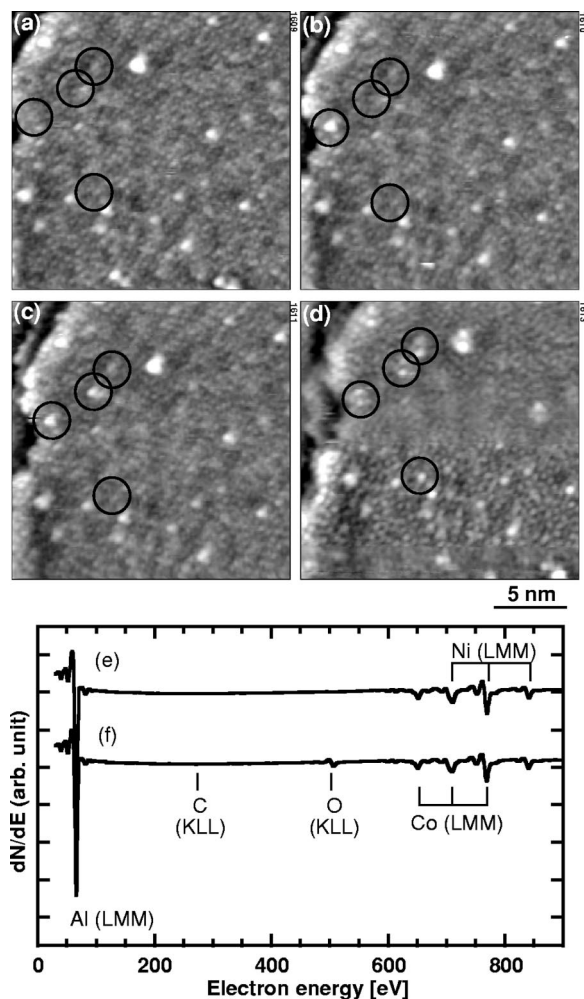
FIG. 6. STM images of the $Al_{72}Co_{16}Ni_{12}$ surface (20×20 nm^2; $I = 0.5$ nA, $V = -0.2$ V) as-prepared (a) and after exposure to O_2 gas at 2×10^{-6} Pa at RT for 1 min (b), 3 min (c), and 6 min (d). Black circles show the positions where protrusions attributed to oxide clusters form. AES spectra of the $Al_{72}Co_{16}Ni_{12}$ surface as-prepared (e) and after exposure to O_2 gas at 2×10^{-6} Pa at RT for 6 min (f).

FIG. 7. STS spectra of the $Al_{72}Co_{16}Ni_{12}$ surface at maxima (circles) and minima (squares) of the STM image of the clean QC surface as well as the features attributed to oxide clusters (triangles). The inset shows the STM image acquired simultaneously ($V = -0.5$ V, $I = 0.5$ nA).

in the first monolayer than in the altered layer below.[25]

The surface concentration of Al after annealing above 750 K was found by ISS to be higher than in the bulk. Again, we attribute the increased Al concentration to its lower surface energy. The surface density of the Al atoms determined by ISS, $(8 \pm 1) \times 10^{14}$ cm^{-2}, agrees well with the adatom density on a decagonal $Al_{71.8}Co_{14.8}Ni_{13.4}$ surface obtained from a He atom diffraction measurement (8×10^{14} cm^{-2}, Ref. 26). The monolayer atomic density in the bulk can be calculated to be 1.4×10^{15} cm^{-2} from the reported atomic density of bulk $Al_{72.6}Co_{16.9}Ni_{10.5}$, 6.9×10^{22} cm^{-3} (4.11 g cm^{-3}, Ref. 27) and the interlayer distance of 0.2 nm.[14,15] This corresponds to 1.0×10^{15} atoms/cm^2 for Al and 0.4×10^{15} atoms/cm^2 for the transition metals. Therefore, the surface atomic density of the transition metals determined from the ISS experiments $[(1 \pm 0.2) \times 10^{14}$ cm$^{-2}]$ is much lower than the atomic density of a truncated bulk. Whereas the ISS result could be explained by a strong inwards buckling of the TM atoms, which would then lie in a plane be-
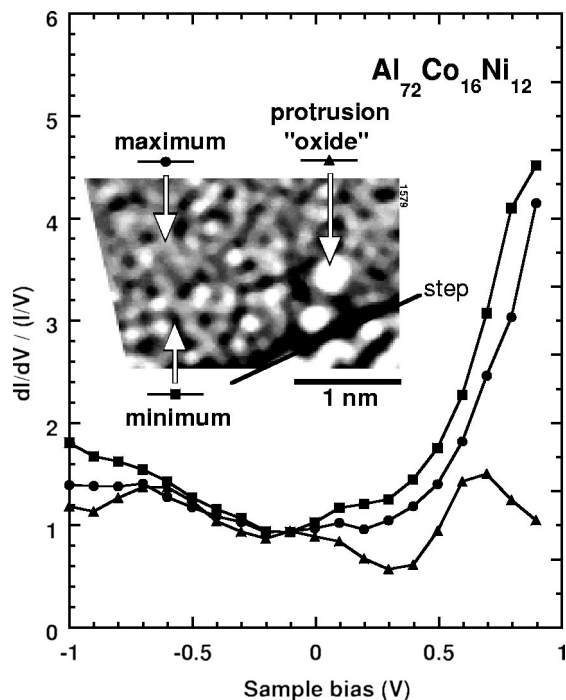
tween the Al layers, such a buckling would leave the AES result of Al enrichment unexplained. Although we cannot completely exclude the possibility of a stoichiometric surface when assuming a large error in the Auger calibration, we consider it more likely that there are true TM vacancies in the surface. This could be favorable if each TM vacancy in the surface uncovers an Al atom in the second layer. The second-layer Al atom has a surface energy much lower than the TM and is also larger (and, thus, geometrically higher) than the average of the second-layer atoms. Since the density of protrusions (maxima) in the STM images, $(8 \pm 1) \times 10^{14}$ cm^{-2}, is the same as the Al surface density, the protrusions in the present QC STM images are considered to correspond to Al atoms only. It has been also reported that STM only images Al atoms on the AlNi(110) surface as protrusions.[20,28]

Figure 8(a) shows a high-resolution STM image of the $Al_{72}Co_{16}Ni_{12}$ surface with a random pentagonal tiling pattern superimposed. The tiling pattern was chosen such that all vertices coincide with fivefold features of the surface (mostly type "A" as defined in Fig. 3). The tiles used are a pentagon, and a skinny and fat rhombus, all with 2 nm edges. This edge length roughly coincides with the cluster size reported in Ref. 11. We have also tried other edge lengths (related by powers of the golden ratio), and got qualitatively similar results. Since we could not find any tiling describing our surface with fat and skinny rhombs only, we had to use the pentagon as a third type of tile. Hence, the QC surface forms a random pentagonal tiling, not an ideal quasiperiodic Penrose tiling. This is consistent with the bulk Co-rich
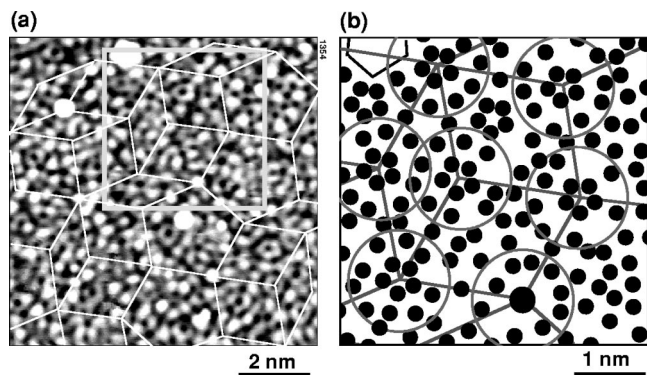
FIG. 8. (a) Random Penrose tiling superimposed on the STM image of the $Al_{72}Co_{16}Ni_{12}$ surface from Fig. 3(a). The ring centers are connected by the five basis vectors with about 2 nm length. (b) Atomic arrangement of the $Al_{72}Co_{16}Ni_{12}$ surface extracted from (a).

Al–Co–Ni QCs which also form a random tiling.[29,30] Furthermore, the surface of the quasicrystal has symmetry different from the Penrose tiling. As mentioned previously, on one terrace of the $Al_{72}Co_{16}Ni_{12}$ QC surface the pentagons of a given size usually have the same orientation. In a Penrose tiling, all features occur in the two orientations related by inversion symmetry. Since an autocorrelation function has inversion symmetry by definition, this difference in symmetry is not reflected in the ACFs. Indeed, we find that the ACF of the STM images, whether such including many terraces like Fig. 2(c) or others derived from single terrace, display the same pattern as the ACF of an ideal Penrose tiling.

Figure 8(b) shows the arrangement of the protrusions attributed to Al atoms on the $Al_{72}Co_{16}Ni_{12}$ surface extracted from the gray square of the STM image Fig. 8(a). The minimum nearest neighbor atomic distance is 0.32 nm, and some of the nearest neighbor distances are more than 0.8 nm. Moreover, all of the decagonal rings are imperfect. If, as discussed above, STM shows only the Al atoms as protrusions, the TM atoms are located probably at the missing positions of the decagonal ring and somewhere in the space in between. This view is supported by the fact that 0.32 nm is larger than the Al–Al distance in bulk Al (0.286 nm). Some TM positions of the ideal QC lattice may be also occupied by Al atoms.

Figure 9(a) shows an atomic structure model of the $Al_{72}Co_{16}Ni_{12}$ surface with perfect decagonal rings. The atomic density in this model is $(9\pm1)\times10^{14}$ cm^{-2}, which is closer to the bulk Al density and hence the atomic arrangement of the model might represent all Al positions in a truncated bulk lattice. The ACF of this model is shown in Fig. 9(b), which is in good agreement with Fig. 2(c). Radially averaged ACFs from STM image and the atomic structure model are shown in Fig. 9(c). The oscillations in both the averaged ACFs of the experimental image and the model have their maxima and minima at the same distances. In contrast to our findings, where the small pentagons are surrounded by larger pentagons or (imperfect) tenfold rings, the recent models of Mihalkovič *et al.*[31] based on total energy minimization contain small Al pentagons surrounded by (more or less perfect) 15-fold rings of Al, at least if the simulation cells are large enough for such structures. We did not find any indications of 15-fold rings, however. Our structure model also differs from the other previous models of the bulk atomic structure.[11,31,35,37,38] It must be mentioned, however, that some of these models[11,34,36–38] were devised for Al–Co–Ni quasicrystals with significantly higher Ni concentration (and, hence lower Co concentration), whereas our quasicrystal is Co-rich.

The number of bright dots (protrusions with $\approx$0.12 nm height) increases in the UHV chamber after a few hours or with exposure to O_2 gas at a pressure of 1.3×10^{-6} Pa for a few minutes at RT. Since the O *KLL* peak in Auger spectra increases after these treatments, these bright dots are attributed to reaction of the QC surface with O atoms from the O_2 gas or H_2O from the residual gas, resulting in formation of small oxide clusters. From our O_2 adsorption experiment, we can estimate that only one out of 10^3 impinging O_2 molecules leads to formation of the bright dot. This means that the bright dots formed from the residual gas cannot be due to O_2 (which has too low impingement rates at the present partial pressure) but must be due to some other species, possibly H_2O. The bias dependence of $(dI/dV)/(I/V)$ of the $Al_{72}Co_{16}Ni_{12}$ QC surface at these bright dots shows much lower conductivity at energies above the Fermi level than that on the clean QC surface. This also indicates that the bright dots are chemically different from the quasicrystal surface.
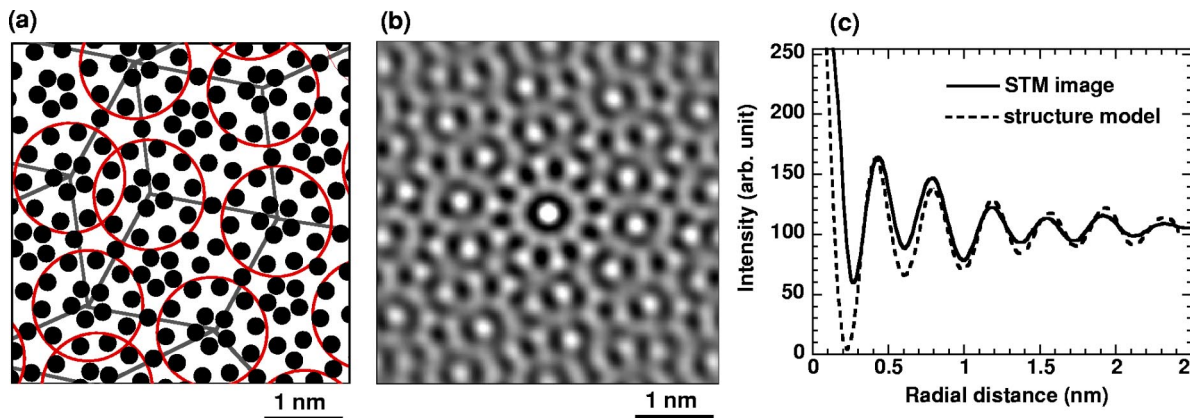

FIG. 9. (a) Idealized model for the arrangement of the Al atoms in the top surface for an $Al_{72}Co_{16}Ni_{12}$ surface. (b) Autocorrelation function (ACF) of (a). (c) Radial distribution of the ACFs from the present experimental STM image and atomic structure model.

V. SUMMARY

We have obtained atomic resolution STM images of the well-characterized decagonal $Al_{72}Co_{16}Ni_{12}$ surface for the first time. In the STM images, we have observed several types of atomic structures of different sizes with the fivefold symmetry and tenfold rings. Locally, a larger ring with 20 protrusions is also observed. The ISS signals, together with the AES ratio between Co and Ni, yield surface densities of Al, Co, and Ni of $(8\pm1)\times10^{14}$ cm^{-2}, $(0.6\pm0.2)\times10^{14}$ cm^{-2}, $(0.4\pm0.2)\times10^{14}$ cm^{-2}, respectively. The Al density is found to be in agreement with the density of maxima in the STM images, indicating that only the Al atoms are observed. Based on the STM images, we have pro- posed a model of the atomic structure. Protrusions of 0.12 nm in height are attributed to oxide clusters from *in situ* STM measurements under O_2 gas and STS-STM measure- ments.

*Corresponding author. Electronic address: j-yuhara@nucl.nagoya- u.ac.jp

[1] A. R. Kortan, R. S. Becker, P. A. Thiel, and H. S. Chen, Phys. Rev. Lett. **64**, 200 (1990).

[2] R. S. Becker, A. R. Kortan, P. A. Thiel, and H. S. Chen, J. Vac. Sci. Technol. B **9**, 867 (1991).

[3] T. M. Schaub, D. E. Burgler, H.-J. Guntherodt, and J. B. Suck, Phys. Rev. Lett. **73**, 1255 (1994).

[4] M. Gierer, M. A. Van Hove, A. I. Goldman, Z. Shen, S.-L. Chang, P. J. Pinhero, C. J. Jenks, J. W. Anderegg, C.-M. Zhang, and P. A. Thiel, Phys. Rev. B **57**, 7628 (1998).

[5] A. P. Tsai, A. Inoue, and T. Masumoto, Mater. Trans., JIM **30**, 150 (1989).

[6] T. J. Sato, T. Hirano, and A. P. Tsai, J. Cryst. Growth **191**, 545 (1998).

[7] Y. Yokoyama, R. Note, S. Kimura, A. Inoue, K. Fukaura, and H. Sunada, Mater. Trans., JIM **38**, 943 (1997).

[8] M. Gräber, R.-U. Barz, P. Dreier, and P. Gille, Mater. Sci. Eng., A **294-296**, 143 (2000).

[9] K. Edagawa, H. Tamaru, S. Yamaguchi, K. Suzuki, and S. Takeu- chi, Phys. Rev. B **50**, 12 413 (1994).

[10] S. Ritsch, C. Beeli, H. U. Nissen, T. Göedecke, M. Scheffer, and R. Lück, Philos. Mag. Lett. **78**, 67 (1998).

[11] K. Hiraga, W. Sun, and A. Yamamoto, Mater. Trans., JIM **35**, 657 (1994).

[12] W. Steurer, T. Hailbach, B. Zhang, S. Kek, and R. Lück, Acta Crystallogr., Sect. B: Struct. Sci. **B49**, 661 (1993).

[13] A. Yamamoto, K. Kato, T. Shibuya, and S. Takeuchi, Phys. Rev. Lett. **65**, 1603 (1990).

[14] M. Gierer, A. Mikkelsen, M. Graber, P. Gille, and W. Moritz, Surf. Sci. Lett. **463**, L654 (2000).

[15] M. Kishida, Y. Kamimura, R. Tamura, K. Edagawa, S. Takeuchi, T. Sato, Y. Yokoyama, J. Q. Guo, and A. P. Tsai, Phys. Rev. B **65**, 094208 (2002).

[16] M. Zurkirch, B. Bollinger, M. Erbudak, and A. R. Kortan, Phys. Rev. B **58**, 14113 (1998).

[17] Ph. Ebert, F. Kluge, M. Yurechko, B. Grushko, and K. Urban, Surf. Sci. **523**, 298 (2003).

[18] V. Fournee, A. R. Ross, T. A. Lograsso, P. Canfield, I. Fisher, J. W. Evans, and P. A. Thiel Surf. Sci. **537**, 5 (2003).

[19] E. J. Cox, J. Ledieu, R. McGrath, R. D. Diehl, C. J. Jenks, and I. Fisher, MRS Symposium Proceedings Volume 643, Quasicrystals- Preparation, Properties and Applications, 2001, K11.3.1–K11.3.6.

[20] M. Schmid and P. Varga, Chap. 4, *The Chemical Physics of Solid Surfaces*, Vol. 10: Alloy surfaces and surface alloys, edited by D. P. Woodruff (Elsevier, New York, 2002), pp. 118–151.

[21] L. E. Davis, N. C. MacDonald, P. W. Palmberg, G. E. Riach, and R. E. Weber, *Handbook of Auger Electron Spectroscopy*, 2nd ed. (Physical Electronics Industries, Eden Prairie, 1976).

[22] C. J. Jenks, T. E. Bloomer, M. J. Kramer, T. A. Lograsso, D. W. Delaney, A. R. Ross, D. J. Sordelet, M. F. Besser, and P. A. Thiel, Appl. Surf. Sci. **180**, 57 (2001).

[23] J. Lindhard, V. Nielsen, and M. Scharff, Mat. Fys. Medd. K. Dan. Vidensk. Selsk. **36**, No. 10 (1968).

[24] F. Shi, Z. Shen, D. W. Delaney, A. I. Goldman, C. J. Jenks, M. J. Kramer, T. Lograsso, P. A. Thiel, and M. A. Van Hove, Surf. Sci. **411**, 86 (1998).

[25] K. Wittmaack, in *Practical Surface Analysis*, edited by D. Briggs and M. P. Seah (Wiley, Chichester, 1992), Vol. 2, p. 103 and references therein.

[26] K. J. Franke, H. R. Sharma, W. Theis, P. Gille, Ph. Ebert, and K. H. Rieder, Phys. Rev. Lett. **89**, 156104 (2002).

[27] Chr. Khoukaz, R. Galler, H. Mehrer, P. C. Canfield, I. R. Fisher, and M. Feuerbacher, Mater. Sci. Eng., A **294-296**, 697 (2000).

[28] K. Højrup Hansen, J. Gottschalck, L. Petersen, B. Hammer, E. Lægsgaard, F. Besenbacher, and I. Stensgaard, Phys. Rev. B **63**, 115421 (2001).

[29] D. Joseph, S. Ritsch, and C. Beeli, Phys. Rev. B **55**, 8175 (1997).

[30] Y. Yan, S. J. Pennycook, and A. P. Tsai, Phys. Rev. Lett. **81**, 5145 (1998).

[31] M. Mihalkovic, I. Al-Lehyani, E. Cockayne, C. L. Henley, N. Moghadam, J. A. Moriarty, Y. Wang, and M. Widom, Phys. Rev. B **65**, 104205 (2002).

[32] S. E. Burkov, Phys. Rev. Lett. **67**, 614 (1991).

[33] A. Yamamoto and S. Weber, Phys. Rev. Lett. **78**, 4430 (1997).

[34] K. Hiraga, T. Ohsuna, W. Sun, and K. Sugiyama, J. Alloys Compd. **342**, 110 (2002).

[35] E. Abe, K. Saitoh, H. Takakura, A. P. Tsai, P. J. Steinhardt, and H.-C. Jeong, Phys. Rev. Lett. **84**, 4609 (2000).

[36] M. Krajcí, J. Hafner, and M. Mihalkovic, Phys. Rev. B **62**, 243 (2000).

[37] H. Takakura, A. Yamamoto, and A. P. Tsai, Acta Crystallogr., Sect. A: Found. Crystallogr. **A57**, 576 (2001).

[38] E. Abe, S. J. Pennycook, and A. P. Tsai, Nature (London) **421**, 347 (2003).